Multiwavelength Interferometry and Competing Optical Methods for the Thermal Probing of Thin Polymeric Films

N. Vourdas,[1,2] G. Karadimos,[1,3] D. Goustouridis,[1] E. Gogolides,[1] A. G. Boudouvis,[2] J.-H. Tortai,[4] K. Beltsios,[3] I. Raptis[1]

[1]*Institute of Microelectronics, National Center for Scientific Research ''Demokritos'', Athens 15310, Greece*
[2]*School of Chemical Engineering, National Technical University of Athens, Zografou 15780, Greece*
[3]*Department of Materials Science and Engineering, University of Ioannina, Ioannina 45110, Greece*
[4]*Laboratoire des Technologies de la Microelectronique, CNRS, 38054 Grenoble, France*

Received 7 March 2006; accepted 12 July 2006
DOI 10.1002/app.25107
Published online in Wiley InterScience (www.interscience.wiley.com).

ABSTRACT: Multiple-wavelength interferometry (MWI), a new optical method for the thermal probing of thin polymer films, is introduced and explored. MWI is compared with two standard optical methods, single-wavelength interferometry and spectroscopic ellipsometry, with regard to the detection of the glass transition temperature (T_g) of thin supported polymer films. Poly(methyl methacrylate) films are deposited by spin coating on Si and SiO_2 substrates. MWI is also applied to the study of the effect of film thickness (25–600 nm) and polymer molecular weight (1.5×10^4 to 10^6) on T_g, the effect of film thickness on the coefficients of thermal expansion both below and above T_g, and the effect of deep UV exposure time on the thermal properties (glass transition and degradation temperatures) of the films. This further exploration of the MWI method provides substantial insights about intricate issues pertinent to the thermal behavior of thin polymer films. © 2006 Wiley Periodicals, Inc. J Appl Polym Sci 102: 4764–4774, 2006

Key words: glass transition; thin polymeric films; spectroscopic ellipsometry; interferometry; coefficient of thermal expansion; poly(methyl methacrylate); lithography

INTRODUCTION

Work on polymeric amorphous thin films is an important part of recent research activity in the polymer-involving area of Applied Nanoscience. The physical, mechanical, and chemical properties of such thin polymeric films are pertinent to a wide range of applications, including semiconductor fabrication (photoresists for micro- and nanolithography and new organic dielectrics), organic light emitting diodes, microsystems, biomicrosystems, pharmaceuticals, etc. (e.g.[1–3]). For the majority of these applications, the polymers are used in the form of thin films supported by a rigid substrate such as silicon (Si). The thermal characteristics of thin polymeric films affect the rate of chemical changes and the evolution of structural features during thin film processing; hence knowledge and understanding of these characteristics is crucial for the precise tailoring of final structures. Thermal properties of thin polymer films deviate frequently and substantially from those of the bulk polymers both because of limited film thickness and interfacial phenomena at the polymeric film/substrate interface; for example, it is now established that the mobility of interface polymer chains is different from that of bulk polymer chains.[4,5] At the same time conflicting reports as regards to the thermal behavior of seemingly similar thin polymer films are far from rare. Glass transition temperature (T_g) is the most characteristic parameter affecting the performance of amorphous thin polymer films for the aforementioned applications. Still, the behavior of thin film T_g is complex and far from fully understood; thus the development of *in situ* methodologies for T_g and related measurements has gained considerable attention.[6,7]

Significant research effort has been devoted to the development of accurate methods for measuring the T_g of polymers,[5,8–11] such as modulated differential scanning calorimetry, dynamic mechanical analysis, thermal mechanical analysis, etc. However, for the T_g measurement of thin films (T_g^{film}), the aforementioned methods cannot be applied, at least in a straightforward manner, and thus alternative techniques are implemented to monitor the temperature-induced changes within the polymeric film. Such new methods include thin film differential scanning calorimetry,[12] scanning viscoelasticity microscopy,[13] X-ray reflectivity (XRR),[14,15] quartz crystal microbalance,[16] spectro-

Correspondence to: I. Raptis (raptis@imel.demokritos.gr).
Contract grant sponsor: More Moore project, EU; contract grant number: IST-1-507754-IP.
Contract grant sponsor: Ministry of Education and Religious affairs, Greece.

scopic ellipsometry (SE),[17] Brillouin light scattering (BLS),[18] local thermal analysis,[15,19,20] ultrasonic,[21] fluorescence monitoring of a dye molecule in a polymer matrix,[22] lateral force microscopy,[23] dielectric spectroscopy,[24] thermal discharge in X-ray photoelectron spectroscopy,[25] single-wavelength interferometry (SWI),[26] and electrical conductivity along with viscosity measurements.[27] From the application of these methods various parameters affecting the T_g^{film} have emerged. Some of those parameters, such as molecular weight (M_w)[28] and tacticity,[28] are familiar from the corresponding cases of bulk films, though the form of dependence may differ. Other parameters, such as film thickness,[17] substrate type,[18] etc. are specific to thin films and also related to the case of glass transition of substances in confined environments of nanoscale dimensions.[29] With regard to the thin-film thickness, the T_g could decrease or increase as film thickness decreases[30–32]; pertinent theory remains incomplete (for example[33]) and surprising experiment findings are far from rare. It must be emphasized that polymeric film thickness issues are extremely important for nanolithography because of the anticipated critical dimension miniaturization within the following years, which will be followed by a further decrease of aspect ratio (polymeric film thickness over minimum pattern dimension) from 3 : 1 to 2 : 1, mostly because of enhanced capillary forces (inversely proportional to the dimensions of the openings) causing the pattern collapse.[34] Consequently, experimental studies for specific films of interest are necessary, especially for chemical systems that are expected to show self-organization behavior. In this context, there have been some attempts to develop empirical and semiempirical schemes to predict the T_g^{film} as a function of film thickness,[17,35] as a function of both film thickness and M_w[36] and as a function of film thickness and density variations.[37]

In many cases, different T_g^{film} values have been reported for the same polymeric system and suggested explanations usually focus on differences in the experimental conditions during the measurement. The complexity of the T_g^{film} metrology is further enhanced by the absence of any relevant engineering standardization. Because of the plethora of different methodologies that have been implemented so far, some studies have been devoted to the comparison and correlation of the results from different techniques, e.g., SE results have been compared with dielectric spectroscopy,[24] BLS,[38] and XRR results.[15]

In this work, three different optical T_g^{film} measurement methodologies are compared through the study of the effects of thickness and processing conditions on the T_g^{film} of poly(methyl methacrylate). The three methods are the previously explored SWI and SE and a new method introduced herein: multiwavelength interferometry (MWI). Emphasis is placed upon MWI, which is further explored as regards to its capacity to probe additional issues pertinent to the thermal characteristics of supported thin polymer films.

EXPERIMENTAL

Materials and sample preparation

Four poly(methyl methacrylate) (PMMA) samples of different molecular weights (M_W) were purchased from Aldrich Chemical Company (1): $M_W = 15{,}000$, (2) $M_W = 120{,}000$, (3) $M_W = 350{,}000$, and (4) $M_W = 996{,}000$. Propylene-glycol-monomethyl-ester-acetate (PGMEA), used for the preparation of the solutions, was also supplied by Aldrich Chemical Company. The substrates used were clean Si wafers with a native oxide of $\sim$1.5 nm in the case of spectroscopic ellipsometry (SE) and single-wavelength interferometry (SWI) and with 1060 nm thermally grown SiO_2 (wet oxidation at 1100°C for 2 h) in the case of multiwavelength interferometry (MWI).

The polymeric films were deposited from solutions on the substrates through spin-coating. Film thicknesses in the range of 25–600 nm are obtained through appropriate choices of polymer concentration and angular velocities. Samples were postapply annealed for 30 min at 160°C in an oven, to evaporate the remaining solvent and then left to cool at room temperature.

Spectroscopic ellipsometry

On the basis of the volume of published works, the SE method is the most currently popular methodology for the T_g^{film} measurement. Ellipsometry measures the change in the polarization state of light as it reflects off a sample surface.[39] This change is expressed as the ratio of the complex Fresnel reflection coefficients r_p and r_s (for light polarized parallel and perpendicular to the plane of incidence). The aforementioned ratio is

$$\rho = \frac{r_p}{r_s} = \tan(\Psi)\, e^{i\Delta} \tag{1}$$

where, $\tan(\Psi)$ is the ratio of the magnitudes of r_p and r_s and Δ is the phase difference between the coefficients. A typical SE spectrum consists of Ψ and Δ angles for every wavelength studied.

For the SE measurements presented herein a J.A. Woollam M2000F rotating compensator ellipsometer (RCE) within the 300–1000 nm spectrum, at an angle of incidence of 75.14°, was employed. Primary data collection and subsequent data processing was accomplished with the commercial WVASE32 software. To *in situ* monitor the Ψ and Δ variation against temperature, the sample stage was properly fixed [Fig. 1 (left)] by employing a hot plate equipped with a PID-pro-

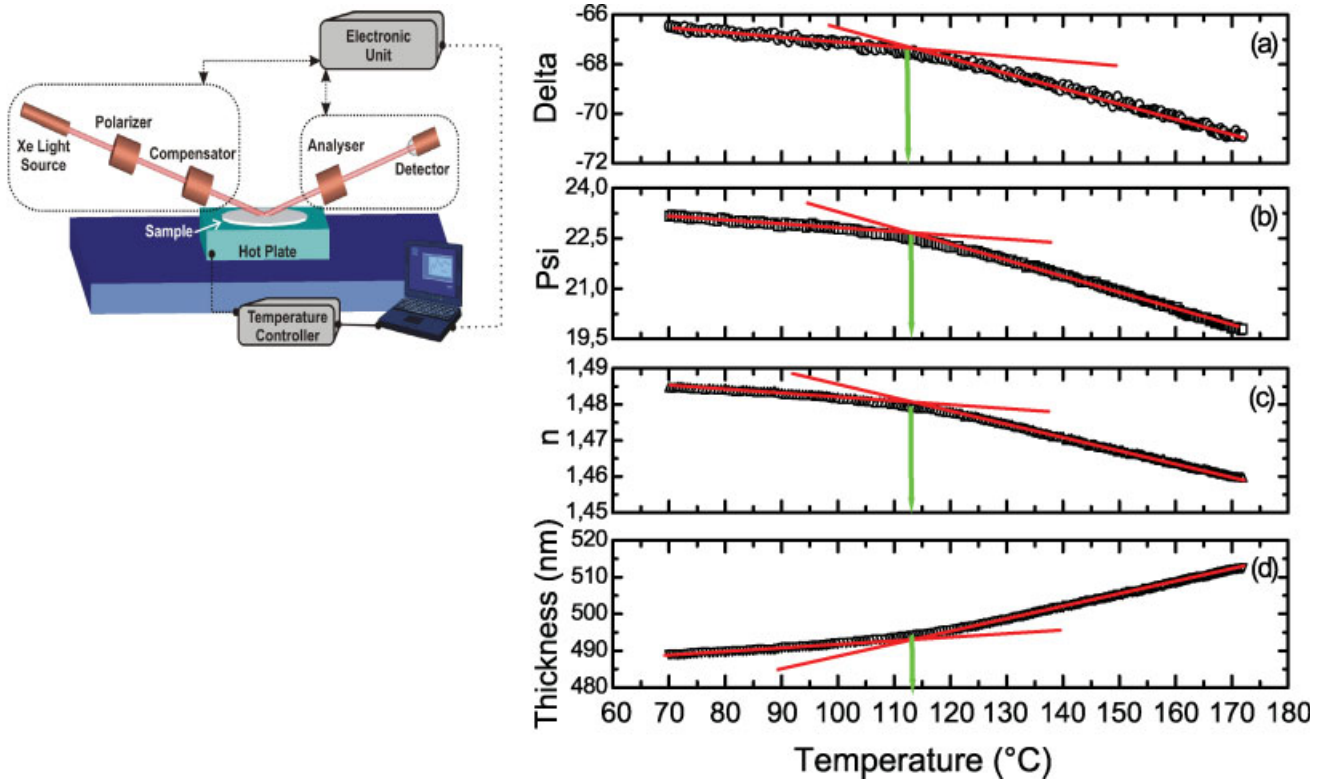

Figure 1 (Left) Schematic of the SE experimental set-up; (right) four different analysis methodologies for T_g evaluation of PMMA ($M_W = 120$K) film by utilizing spectroscopic ellipsometry. In (a) and (b) the T_g^{film} is defined by the change of the slope of Δ and Ψ (both at 691 nm) versus temperature respectively. In (c) and (d) T_g^{film} is determined by the change of the slope of n and film thickness versus temperature. In all cases (a–d) the T_g^{film} is identical. [Color figure can be viewed in the online issue, which is available at www.interscience.wiley.com.]

grammable controller. The hot plate temperature is automatically recorded by utilizing a thermocouple located very close to the plate/sample interface and its signal feeds the controller to achieve the desirable heating conditions and, unless stated otherwise, the heating rate was $\sim 20^\circ$C/min. In a typical case, the T_g^{film} value can be readily determined based on those primary data [Figs. 1(a) and 1(b)]. Since glass transition is accompanied by a change in the coefficient of thermal expansion (CTE) and the refractive index, the change in the slope of Ψ or Δ curve versus temperature indicates the transition from the glassy to the viscoelastic phase. To locate exactly the T_g^{film} value, we employed three methodologies:

- (a) A plain linear fitting as employed by many scientific studies (e.g.,[17,40])
- (b) A more systematic procedure summarized as follows: estimate approximately (by plain extrapolation) an approximate T_g^{film} value, then ignore all points within $\pm 15^\circ$C from the calculated value and use the remaining for least square fittings and drawing of two intersecting straight lines. Thus a new T_g value is determined and the procedure is repeated until two successive values determined are practically identical ones.
- (c) The third methodology makes use of an equation introduced by Dalnoki-Veress et al.[38]

Pertinent issues are discussed in the section T_g Estimation through MWI, SWI, and SE. All three methodologies result, in most cases, in approximately the same values; further, the trends extracted by the three methodologies are identical.

Finally we have also applied to representative sets of data another procedure[41] and obtained T_g values very close to the ones reported herein.

The prime advantage of this methodology is that additional physicochemical information can be extracted through analysis of the primary Ψ and Δ data. SE is widely used to readily determine both film thickness and index of refraction independently[39]; still, pertinent determination becomes difficult when film thickness drops to the nanorange, since the dielectric function of the material may be completely different from the bulk. To treat this predicament, Arwin and Aspnes[42] have proposed an analysis procedure, which is also adopted throughout this work.

To analyze Ψ and Δ, a Cauchy dispersion model $\left[n = A + \frac{B}{\lambda^2} + \frac{C}{\lambda^4}\right]$ was assumed for the polymeric layer with refractive index (n) [namely A, B, C] and film thickness (d) as fitted parameters. The results for the

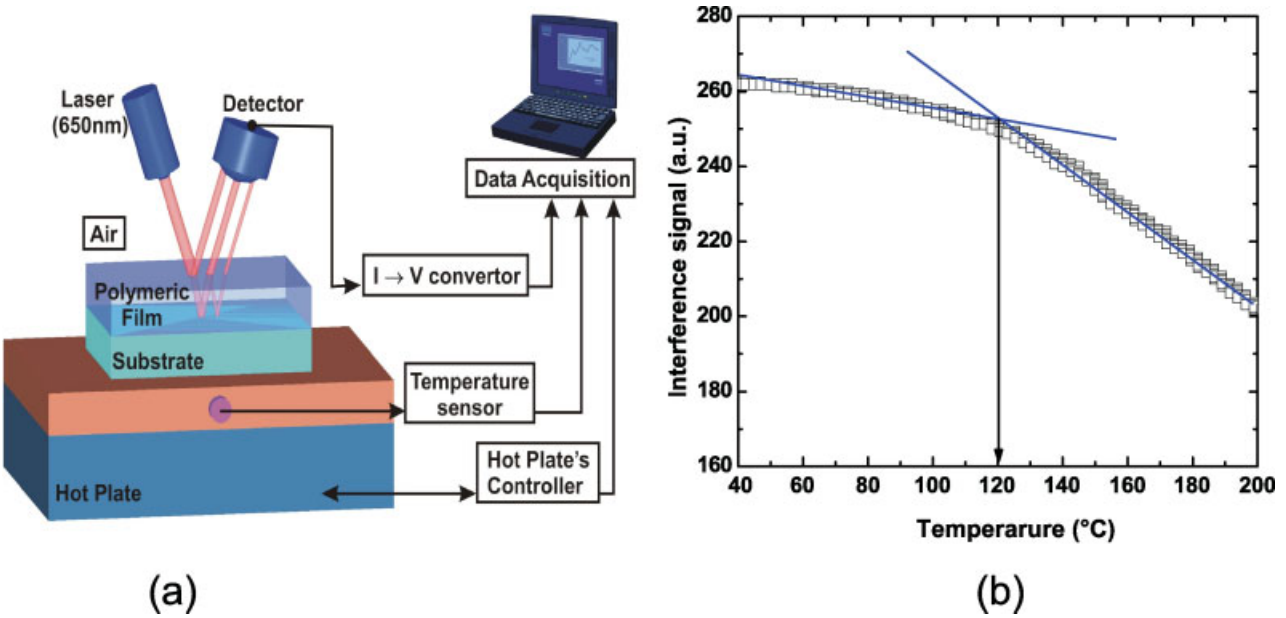

Figure 2 (a) Schematic of the in-house SWI experimental set-up, and (b) a typical profile of the primary raw data; interference signal against temperature. The analysis of these data based on linear fitting is also illustrated. [Color figure can be viewed in the online issue, which is available at www.interscience.wiley.com.]

case of PMMA (M_W = 120K) 490-nm-thick film is reported in Figures 1(c) and 1(d).

Single-wavelength interferometry

Various aspects of the SWI methodology are described in detail elsewhere[26]; here we will briefly outline the experimental set-up and the principle of operation. In Figure 2(a), a schematic of the in-house experimental set-up is presented. The SWI set-up consists of a laser source, a detector, a data acquisition card, a thermal unit (hot plate) equipped with a temperature controller, and a PC for the data processing and apparatus control. The laser emission wavelength selected for our studies was 650 nm, at which the absorption of our spin-coated polymers is negligible. The sample is placed on the hot plate and the light beam from the laser source meets the polymeric film surface at a nearly 90° angle. The total energy incident on the detector could be approximated as the sum of the energy from two beams, i.e., the contribution of the native SiO_x layer as also the internal reflections in the polymeric films are neglected. One beam (A) comes from the polymeric film surface and the second (B) from the polymeric-film–silicon-substrate interface. The total energy E that reaches the detector could be approximated as[43]

$$E = r_{01}^2 + r_{12}^2 + 2r_{01}r_{12}\cos\left(\frac{4\pi n_1}{\lambda}d_1\right) \tag{2}$$

where

$$r_{01} = \frac{n_0 - n_1}{n_0 + n_1} \tag{2a}$$

$$r_{12} = \frac{n_1 - n_2}{n_1 + n_2} \tag{2b}$$

are the relative refractive indices between adjacent layers (0 is considered as ambient, 1 the polymeric film, 2 the substrate), n_1 the refractive index and d_1 the thickness of the polymeric film respectively, while n_2 the refractive index of the substrate, and λ the corresponding laser wavelength used for the measurement.

The method is based on the fact that at T_g the CTE and the refractive index of the polymeric film undergo a change that results in a change of slope at the interference signal versus temperature graph (heating rate $\sim 20^\circ$C/min). In Figure 2(b), a typical set of raw data is displayed, along with the linear fitting procedure, which is employed to calculate the T_g^{film}.

Multiwavelength interferometry

The MWI methodology resembles SWI but involves, instead of a laser (single wavelength), a VIS-NIR light source (Avantes AvaLight HAL Tungsten-Halogen) and a PC-driven two channel VIS-NIR miniaturized spectrometer (Ocean Optics SD2000) instead of a photodetector [Fig. 3(a)]. In particular, a splitter optical fiber is connected to the light source and is equally split to two beams: one directed to the slave

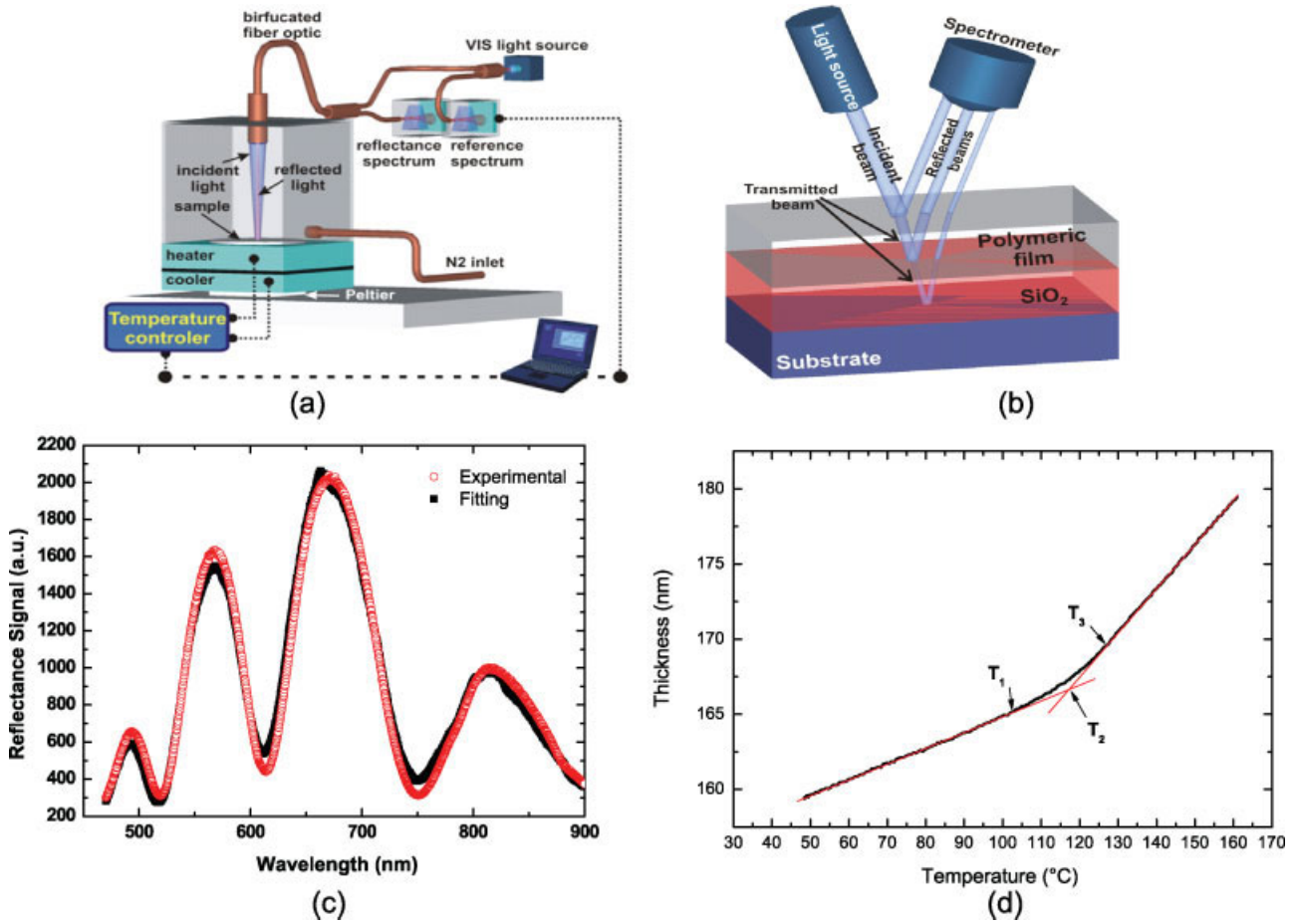

Figure 3 Schematic of (a) the in-house MWI experimental set-up and (b) principle of operation. (c) A typical profile of the primary raw data from one temperature along with the results from the fitting procedure through which the thickness is determined, and in (d) a typical thickness versus temperature graph based on data such as those in (c). The determination of T_g^{film} using linear fitting is also indicated. T_1 and T_3 are the temperatures at which the linearity is lost and T_2 is the T_g^{film}. Throughout this study the T_g^{film} determination via MWI follows this rule. [Color figure can be viewed in the online issue, which is available at www.interscience.wiley.com.]

channel of the double spectrophotometer and another connected to a bifurcated optical fiber. The bifurcated optical fiber then guides the white light onto an appropriate reflective substrate spin-coated with a thin polymer layer. At the same time the bifurcated optical fiber collects the reflected beam, directing it to the master channel of the spectrophotometer. Each channel of the spectrophotometer is sensitive in the VIS-NIR spectrum with a resolution of ~ 0.4 nm. The heating process control is attained through a device assembly similar to that for SWI and is controlled to within 0.5°C, while the whole apparatus is controlled through software developed within the LabView platform. A controlled atmosphere chamber is employed for the purpose of achieving a controlled environment mainly by nitrogen purging. Again, the beam from the light source interacts with the sample [Fig. 3(b)] and produces a reflectance signal that is continuously recorded, in the 470–740 nm range, from a spectrometer during heating.

The substrate should be totally reflective, at the spectrum used. Therefore standard silicon wafers constitute a reasonable choice. The accuracy of the method depends on the number of interference fringes in the recorded spectrum, as the existence of these extrema allows precise fitting of the recorded spectrum and thus accurate calculation of the polymeric film thickness. In the case of thin polymeric films (e.g., 100 nm) on bare Si substrate no extrema appear on the reflectance spectrum. To obtain an adequate number of fringes within the reflectance spectrum, a thick dielectric layer should be added in the film stack. With the Si processing it is easy to either grow a SiO_2 layer or deposit a Si_3N_4 film. In our study the film stack includes thermally grown SiO_2 (wet oxidation at 1100°C for 200 min; final SiO_2 thickness, 1060 nm) on the Si substrate, prior to spin coating of the polymeric film. While this intermediate layer increases the number of interference fringes [Fig. 3(c)], it also provides an accurate and reproducible substrate for the T_g^{film} measurements.

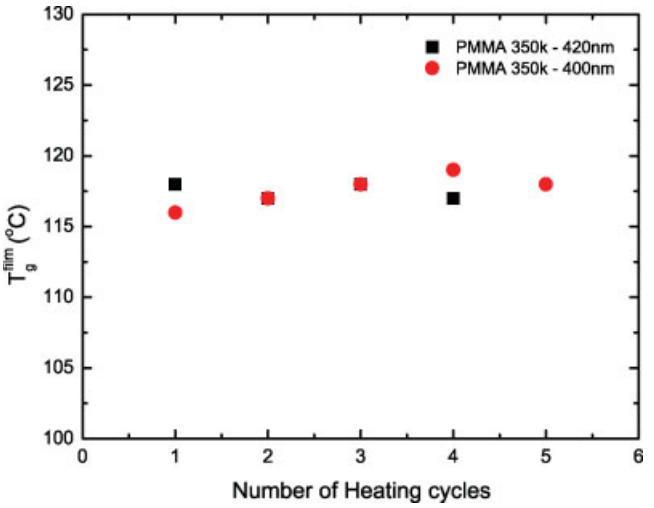

Figure 4 Effect of the number of heating cycles on the T_g of PMMA (M_W = 350K) films. No significant change of T_g^{film} was recorded for up to 5 heating cycles. [Color figure can be viewed in the online issue, which is available at www.interscience.wiley.com.]

The energy that incidents on the spectrometer can be expressed as

$$E = \frac{A}{B} \tag{3}$$

where

$$A = r_{01}^2 + r_{12}^2 + r_{23}^2 + 2r_{01}r_{12}^2r_{23} + r_{01}^2r_{12}^2r_{23}^2 + 2r_{01}r_{23}\cos\left[\frac{4\pi}{\lambda}(n_1 - d_1 + n_2d_2)\right] + 2r_{01}r_{12}r_{23}^2 \times \cos\left[\frac{4\pi}{\lambda}n_2d_2\right] + 2r_{01}r_{12}\cos\left[\frac{4\pi}{\lambda}n_1d_1\right] + 2r_{01}^2r_{12}r_{23}\cos\left[\frac{4\pi}{\lambda}n_1d_1\right] \tag{3a}$$

$$B = 1 + r_{01}^2r_{12}^2 + r_{01}^2r_{23}^2 + r_{12}^2r_{23}^2 + 2r_{12}r_{23} \times \cos\left[\frac{4\pi}{\lambda}n_2d_2\right] + 2r_{01}r_{23}\cos\left[\frac{4\pi}{\lambda}(n_1d_1 + n_2d_2)\right] + 2r_{01}^2r_{12}r_{23}\cos\left[\frac{4\pi}{\lambda}n_2d_2\right] + 2r_{01}r_{12}\cos\left[\frac{4\pi}{\lambda}n_1d_1\right] + 2r_{01}r_{12}r_{23}^2\cos\left[\frac{4\pi}{\lambda}n_1d_1\right] + 2r_{01}r_{12}^2r_{23} \times \cos\left[\frac{4\pi}{\lambda}(n_1d_1 - n_2d_2)\right] \tag{3b}$$

and

$$r_{01} = \frac{n_0 - n_1}{n_0 + n_1} \tag{3c}$$

$$r_{12} = \frac{n_1 - n_2}{n_1 + n_2} \tag{3d}$$

$$r_{23} = \frac{n_2 - n_3}{n_2 + n_3} \tag{3e}$$

are the relative refractive indices between adjacent layers (0 is considered as ambient, 1 the polymeric film, 2 the SiO_2 layer, and 3 the Si substrate), n_1, n_2, and n_3 the refractive indices of the polymeric film, the silicon oxide, and Si substrate respectively, d_1, d_2 the thickness of the polymeric film and the silicon dioxide, and λ the corresponding wavelength.

Thus the thickness of the polymeric film may be calculated by fitting the above-mentioned equation to the experimental interference signal. In Figure 3(d) we demonstrate a typical layer thickness versus temperature graph and the standard linear-fitting method for the T_g^{film} determination (for all samples studied heating rate was ~ 20°C/min). As shown in Figure 3(d), there are two linear regions, the intersection of which corresponds to the point of the transition. The inability to simultaneously determine the thickness and the refractive index variation versus temperature constitutes an inherent weak point of this method. To deal with this problem, one has to assume a constant refractive index and ascribe all interference frequency differences to thickness changes. However, the calculated thickness being lower than the real one, the changes in the slope of layer thickness versus temperature profile are rather sharp and accurate T_g^{film} estimation remains possible.

RESULTS AND DISCUSSION

Basic MWI assessment

In Figure 4 we present T_g^{film} values versus heating cycles, thus showing the reproducibility of MWI methodology. For both polymeric films studied a total deviation of less than 4°C was recorded for up to five heating cycles. This finding may be pertinent to all

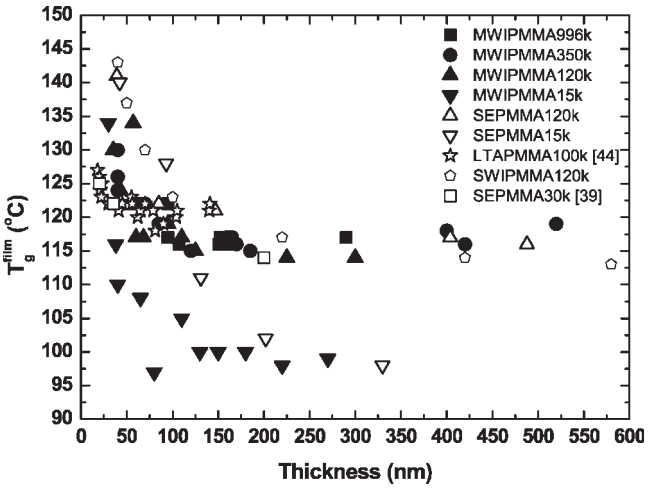

Figure 5 Film thickness effect on PMMA T_g^{film} via MWI and SE. For comparison purposes results from SWI measurements,[26] SE,[40] and local thermal analysis[44] are also portrayed. Errors of T_g values of our measurements are always smaller than ±5°C for films thinner than 50 nm and smaller than ±2°C for thicker films.

TABLE I
T_g Values of Thick Polymeric Films and T_g Values of Bulk Material Measured by SWI, MWI, SE, and DSC (by Approximately the Same Heating Rate)

PMMA	SWI	MWI	SE	DSC
15 K		98	98	87
120 K	114	114	115	113
350 K		117		122
996 K		117		119

glassy polymers for which T_g and the lower end of degradation range are spaced apart by a minimum of 70–100°C (~85°C for a-PMMA), in which case samples can be repeatedly annealed without problem to a temperature exceeding T_g by, say, 20–50°C.

T_g estimation through MWI, SWI, and SE

T_g^{film} is determined for various PMMA molecular weights and various film thicknesses in the range of 25–300 nm; 10–15 thickness values per M_w are explored. Data obtained along with literature values from another method (local thermal analysis, LTA[44]) are presented in Figure 5. Also, bulk T_g values (plateau mean values) through the same methods, along with corresponding DSC values, are presented in Table I. Good agreement between the three optical methods, as well as with LTA, is observed for all molecular weights and thicknesses (Fig. 5). A clear trend of increasing T_g values for low thicknesses is notable and will be discussed in detail subsequently.

With regard to the bulk values reported in Table I a satisfactory agreement between the different methods is observed, with the exception of the 15K, for which the DSC method gives a value that is 11°C lower than that determined through optical methods. The reason for this difference is unclear though not uncommon when T_g values obtained from different methods are compared.[45]

Figure 5 includes the T_g^{film} values of PMMA films (M_W = 15K and 120K) through the SE method. Even though the assessment of T_g^{film} through linear fitting (a procedure used for Fig. 5 data) turns out to be a fast and adequate way of determination, it does not provide any other physical information on the system under study. As an alternative interpretation procedure, Dalnoki-Veress et al.[38] proposed the following scheme to fit the thickness versus temperature data:

$$e(T) = w\frac{M-G}{2}\ln\left(\cosh\left(\frac{T-T_g}{w}\right)\right) + (T-T_g)\frac{M+G}{2} + c \quad (4)$$

where $e(T)$ is the thickness at temperature T (in K), w the glass transition width (in K), M and G are the coefficients of thermal expansion (CTE) of the melt and glass state respectively, (in nm/K), and c the film thickness at the glass transition (in nm).

Although eq. (4) fits well to the experimental data and provides additional physicochemical information [Fig. 6(a)], its results do not exactly coincide with the results obtained through linear fitting (namely the plain linear fitting method presented in the experi-

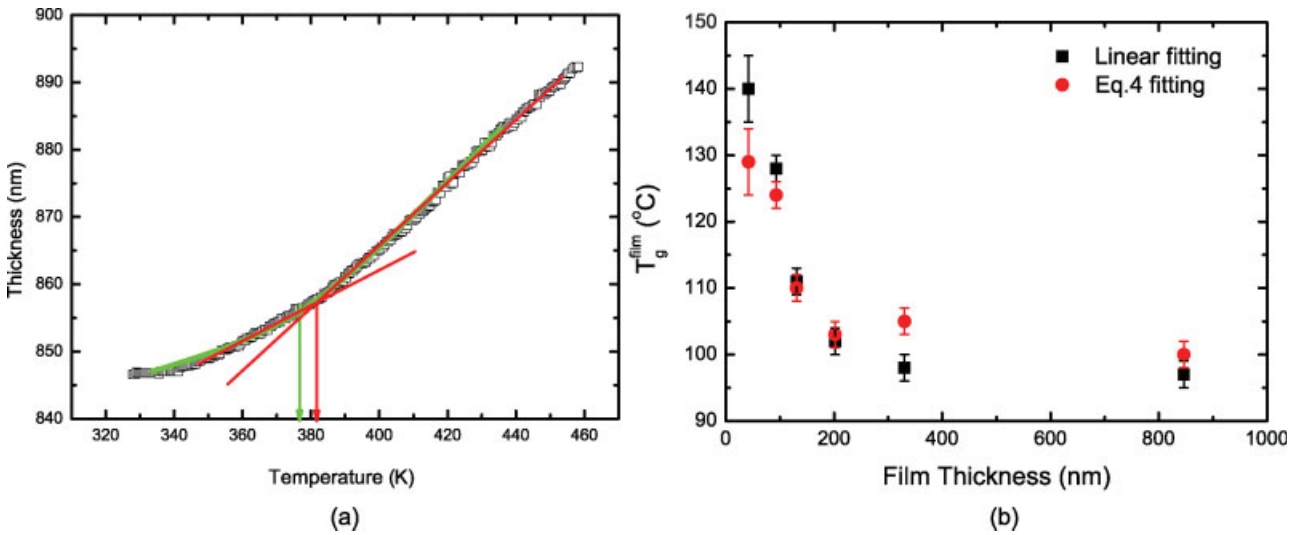

Figure 6 (a) T_g^{film} determination of PMMA 15K film based on data extracted from SE measurements. Two distinct methods are employed: (red line) linear fitting and (green line) eq. (4) fitting. (b) T_g of PMMA (M_W = 15K) films versus thickness based on SE measurements—thickness versus temperature data—(■) by applying linear fitting and (●) by applying eq. (4). [Color figure can be viewed in the online issue, which is available at www.interscience.wiley.com.]

TABLE II
Comparison of the Three Optical Methodologies

	SWI	MWI	SE
Set-up integration	High	High	Low
Cost	Low	Moderate	High
Ease of data interprentation	High	High	Low
Flexibility	High	High	Low
Minimum film thickness	40 nm (with some difficulty)	40 nm (easily)	40 nm (easily)
Discrimination between glass transition and other thermal changes	No	Yes	Yes[a]
Thermal expansion monitoring of thin films (CTE)	Not possible	Approximate	Accurate
Special characteristics		Need for a thick optically transparent layer between substrate and polymeric film	Accurately measured thickness and optical indices

[a] Not an SE problem when monitoring thickness or refractive index. Problem occurs when SE is applied through ellipsometric angles monitoring.

mental section) for films thinner than $\sim$ 70 nm. For film thicknesses higher than $\sim$ 70 nm [see Fig. 6(b)] the two procedures give approximately the same results (within $\pm 3^{\circ}$C).

Preceding discussion and overall experience from the application of the three optical methods considered herein (MWI, SWI, and SE) allow for the comparison presented in Table II.

Coefficients of thermal expansion for thin polymer films

The CTE is determined by the MWI method for each available molecular weight and a thickness in the range 25–500 nm both below and above T_g. Data shown (Fig. 7) pertain to a $M_W = 350$K. Bulk CTE values according to the literature[46] are $\sim 6 \times 10^{-4}$ for $T > T_g$ and 2.5 ($\pm$0.5) $\times 10^{-4}$ for $T < T_g$. Our data suggest that for a thickness up to $\sim$ 100 nm (i.e., similar to the critical thickness according to the previous discussion) both below and above T_g the corresponding glassy and viscoelastic phases are substantially less mobile (lower CTE values) than the bulk phases, while the peak on the right graph (for a thickness of $\sim$ 100 nm) suggests that the viscoelastic phase is the first one that gains additional mobility, typical of the bulk viscoelastic phases. For a thickness more than 100–125 nm the ratio of CTE values reaches the range of bulk values, though individual values remain below the corresponding bulk ones for a thickness up to $\sim$ 400–500 nm. Such details reveal the substantial complexity of glass transition phenomena in thin polymeric films.

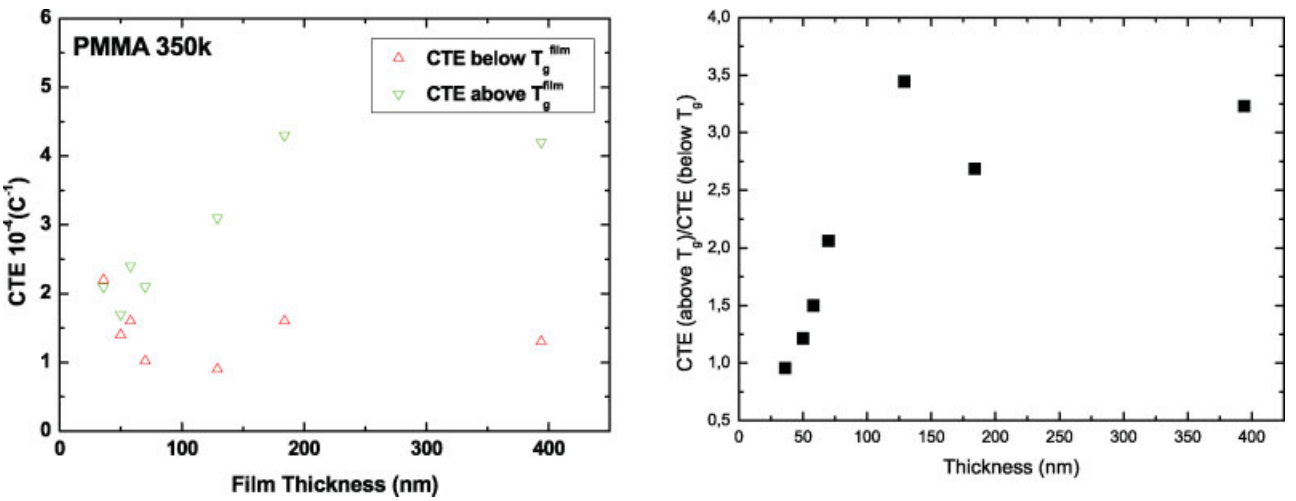

Figure 7 (a) Variation of CTE both below and above T_g as a function of film thickness. (b) Variation of CTE ratio (above T_g/below T_g) as a function of film thickness. This ratio is in the order of 2.5 to 3 for bulk samples, i.e., values in the bulk range are observed for a film thickness exceeding 100–125 nm. [Color figure can be viewed in the online issue, which is available at www.interscience.wiley.com.]

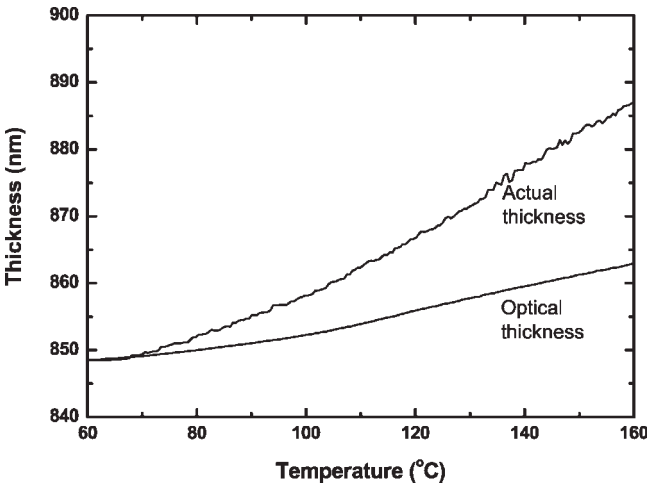

Figure 8 The effect of the thermo-optical coefficient on the CTE. Two extreme cases are shown: (a) actual thickness expansion and (b) optical thickness profile for the case where the thermo-optical coefficient has been set as 0. The optical thickness is always lower than the actual.

On the other hand, SE provides the opportunity to independently extract the thermo-optical coefficient. In Figure 8 we report SE results for both the actual thickness by fitting the refractive index at every temperature (as in Fig. 8) and the nominal thickness by assuming that the thermo-optical coefficient is 0 [as in Fig. 3(c), 3(d)]. A discrepancy with regard to the thickness can be detected, unambiguously; this discrepancy vanishes near room temperature.

Critical thickness for strong polymer–substrate interaction

This section focuses on MWI-derived data for the T_g^{film} versus thickness for a-PMMA of four different M_w values. From Figure 5 we see that T_g^{film} is approximately independent of M_W down to a certain critical thickness, beyond which it starts rising. A plot of the critical thickness versus $(M_W)^{1/2}$ of PMMA is shown in Figure 9. Although the limited number of available M_W and the absence of monodispersity do not permit quantitative claims to be made, a qualitative, at least, conformity of our data to a $M_W{}^{1/2}$ dependence of critical thickness for up to moderate M_W is hinted, in accordance with the results in Ref. [38]. The suggested $M_W{}^{1/2}$ dependence should be viewed as a reflection of the same dependence of the end-to-end chain distance and related quantities. PMMA is capable of attaching strongly to SiO_2 surfaces. Attachment takes place through multiple hydrogen bonding between the carbonyl groups of the chains and the hydroxyl groups of the silicon dioxide surface.[47] This attachment reduces the mobility of chains having immediate access to the substrate surface and, possibly, also the mobility of chains immediately entangled to the first layer of chains. When thickness exceeds a dimension proportional to $M_W{}^{1/2}$ range (where chains influenced by the presence of the substrate are found), the bulk T_g value prevails. The fact that the critical thickness appears to cease being dependent on M_W for rather high M_W values can be, broadly speaking, viewed as another example of the widely documented upper cut-off dimension in the range of ~100 nm for nanoscale phenomena. The additional fact that the extrapolation of the curve on the low side does not pass through the (0,0) point should be attributed to the loss of polymeric characteristics (e.g., Gaussian contours and presence of a substantial level of entanglements) for samples of very low molecular weights.

Glass transition and degradation temperatures upon deep UV exposure

PMMA film samples of various molecular weights and thicknesses are exposed to deep UV (DUV) (200–250 nm) radiation for times ranging from 40 s to 1 h (3600 s); subsequently, the thickness of the samples as a function of temperature is probed by the MWI method. For the DUV exposures a broadband Hg–Xe lamp (Oriel) was used. In addition to the T_g^{film}, another, higher, temperature (T_{degrad}) corresponding to the point of deviation from linearity is recorded [Fig. 10(a)]. The downward deviation from linearity implies that upon heating, a fraction of the material that was part of the sample escapes in the vapor phase, so that less material is left to expand upon further increase of the temperature. Additional tests (not shown) verify that the escaping material is not related to solvent leftovers; that is, the escaping species are volatile products of PMMA degradation. Obviously, T_{degrad} is only a shorthand notation for the actual, more complex situation. The deviation from linearity is a reflection of the temperature at which small mole-

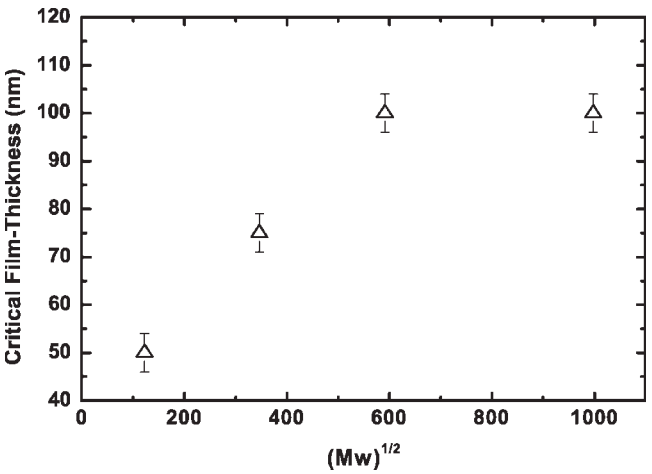

Figure 9 Critical film thickness as a function of PMMA molecular weight (see text for details).

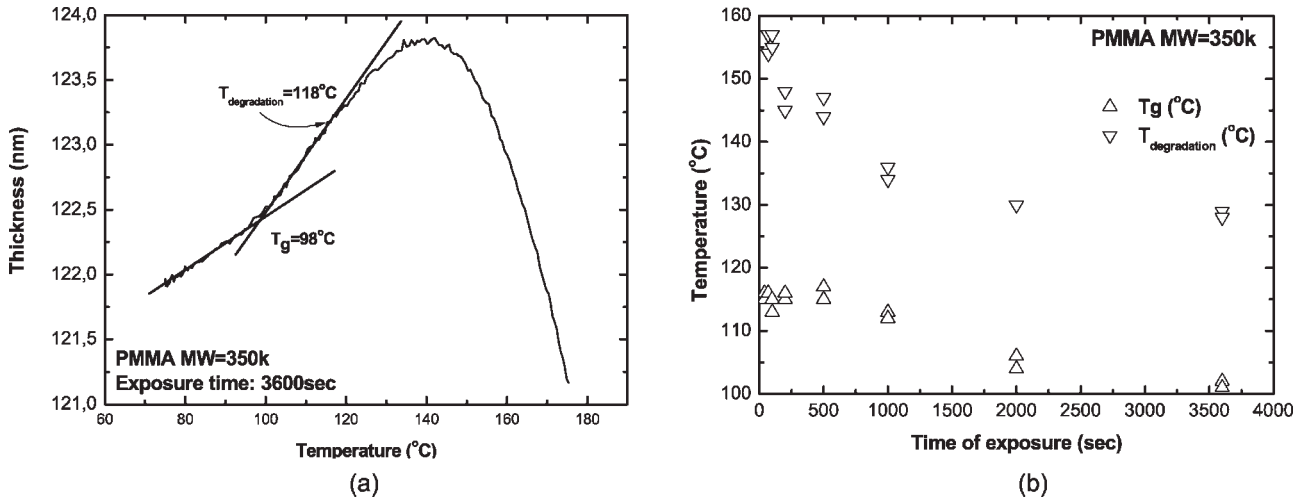

Figure 10 (a) Sample graph of thickness versus temperature for a 350K sample (~120 nm) irradiated for 1 h. (b) Glass transition and degradation temperatures determined as in (a), for a 350K samples irradiated for times ranging from 40 s to 1 h.

cules start to escape massively. While some of the latter products might result from degradation at $T > T_g^{film}$ of chains sensitized during irradiation, part of the sample has already been decomposed during the irradiation step, since the parallel lowering of the corresponding T_g^{film} value is most probably a reflection of the presence of low molecular weight products.

Data for a particular thickness and M_W (~ 120 nm and 350K respectively) and various exposure times are shown in Figure 10(b). It is clear that both characteristic temperatures (T_g^{film} and T_{degrad}) tend to drop with increasing exposure times. The tendencies for very short and very long exposure times are of interest.

For short times the T_g^{film} value tends to level off to the ordinary value for unexposed samples (~ 118 °C for the particular samples). On the other hand, T_{degrad} appears to change dramatically in the range of short exposure times. It can be postulated that the limit for zero exposure time lies in the range of 250°C. No such temperatures can be probed with the set-up in use, but tests for heating up to ~ 200°C showed no degradation for the particular samples and heating rates involved, while literature suggests that PMMA chains undergo an unzipping reaction (leading to oligomeric and monomeric products) at temperatures in the range of 200–250°C ([45] and references therein). In addition, extrapolation of our data to zero exposure time is compatible with a T_{degrad} in the range of 250°C.

For long exposure times (≥ 2000 s), there appears to be a tendency for a leveling off of the T_{degrad} and T_g values. For the case of T_{degrad} some type of equilibrium between unzipping and chain reformation offers the simplest possible explanation (though more complex interpretations are possible). The same explanation would then render a roughly fixed composition and, hence, a fixed T_g value.

CONCLUSIONS

MWI is a new flexible optical method for the probing of thermal properties of thin polymer films. MWI characteristics include set-up integration, ease of data interpretation, lack of false detection of glass transition and probing of thicknesses at least down to 40 nm.

For a polymer film thickness up to ~ 100 nm the glassy and viscoelastic phases are substantially less mobile than the bulk phases, while the viscoelastic phase is the first one that gains additional mobility, typical of the bulk viscoelastic phases.

For a-PMMA on a SiO_2 substrate the T_g^{film} is approximately independent of M_W down to a certain critical thickness, beyond which it starts rising. Critical thickness is found proportional to $M_w^{1/2}$ if not exceeding 100 nm.

During DUV exposure of a-PMMA thin films both T_g and T_{degrad} initially drop with increasing exposure times but tend to level off after a certain exposure dose.

References

1. Shirota, Y. J Mater Chem 2000, 10, 1.
2. Doi, H.; Kinoshita, M.; Okumoto, K.; Shirota, Y. Chem Mater 2003, 15, 1080.
3. Niu, Y.-H.; Hou, Q.; Cao, Y. Appl Phys Lett 2002, 81, 634.
4. Mayes, A. M. Macromolecules 1994, 27, 3114.
5. Lin, E. K.; Wu, W. I.; Satija, S. K. Macromolecules 1997, 30, 7224.
6. Anderson, P. W. Science 1995, 267, 1615.
7. Roth, C. B.; Dutcher, J. R. J Electroanal Chem 2005, 584, 13.
8. Armeniades, C. D.; Baer, E. In Introduction to Polymer Science and Technology; Kaufman, H. S., Falcetta, J. J., Eds.; Wiley Interscience: New York, 1977; Chapter 6.
9. Nielsen, L. E. Mechanical Properties of Polymers and Composites, Vols. I and II; Marcel Dekker: New York, 1974.

10. Rodriguez, F. Principles of Polymer Systems; McGraw-Hill: New York, 1970.
11. Jean, Y. C. Microchem J 1990, 42, 72.
12. Efremov, M.; Warren, J. T.; Oison, E. A.; Zhang, M.; Kwan, A. T.; Allen, L. H. Macromolecules 2002, 35, 1481.
13. Satomi, N.; Takahara, A.; Kajiyama, T. Macromolecules 1999, 32, 4474.
14. Wallace, W. E.; Vanzanten, J. H.; Wu, W. L. Phys Rev E: Stat Phys Plasmas Fluids Relat Interdiscip Top 1995, 52, R3329.
15. Fryer, D. S.; Peters, R. D.; Kim, E. J.; Tomaszewski, J. E.; de Pablo, J. J.; Nealy, P. F. Macromolecules 2001, 34, 5627.
16. Forest, J. A.; Svanberg, C.; Revesz, K.; Rodahl, M.; Torell, L. M.; Kasemo, B. Phys Rev E: Stat Phys Plasmas Fluids Relat Interdiscip Top 1998, 58, R1226.
17. Keddie, J. L.; Jones, R. A. L.; Cory, R. A. Europhys Lett 1994, 27, 59.
18. Forrest, J. A.; Dalnoki-Veress, K.; Stevens, J. R.; Dutcher, J. R. Phys Rev Lett 1996, 77, 2002.
19. Fryer, D. S.; Nealey, P. F.; de Pablo, J. J. J Vac Sci Technol B 2000, 18, 3376.
20. Fischer, H. Macromolecules 2005, 38, 844.
21. Morton, S. L.; Degertekin, F. L.; Khuri-Yakub, B. T. Appl Phys Lett 1998, 72, 2457.
22. Raja, R. A.; Raju, B. B.; Vardarajan, T. S. J Appl Polym Sci 1994, 54, 827.
23. Kajiyama, T.; Kaeaguchi, D.; Sakai, A.; Satomi, N.; Tanaka, K.; Takahara, A. High Perform Polym 2000, 12, 587.
24. Hartmann, L.; Gorbatschow, W.; Hauwede, J.; Kremer, F. Eur Phys J E 2002, 8, 145.
25. Erichsen, J.; Dolgner, K.; Zaporojtchenko, V.; Faupel, F. Macromolecules 2004, 37, 8813.
26. Diakoumakos, C. D.; Raptis, I. Polymer 2003, 44, 251.
27. Koike, T. J Appl Polym Sci 1993, 50, 1943.
28. van Krevelen, D. W. Properties of Polymers, 3rd ed.; Elsevier: Amsterdam, 1990.
29. Zang, J.; Liu, G.; Jonas, J. J Phys Chem 1992, 96, 3478.
30. Kim, J. K.; Jang, J.; Zin, W.-C. Langmuir 2001, 17, 2703.
31. See, Y.-K.; Cha, J.; Chang, T.; Ree, M. Langmuir 2000, 16, 2351.
32. van Zanten, J. H.; Wallace, W. E.; Wu, W. L. Phys Rev E: Stat Phys Plasmas Fluids Relat Interdiscip Top 1996, 53, R2053.
33. de Gennes, P. G. Eur Phys J E 2000, 2, 201.
34. Peters, L. Semicond Int 2005, 28, 38.
35. Kim, J. H.; Jang, J.; Zin, W.-C. Langmuir 2000, 16, 4064.
36. Singh, L.; Ludovice, P. J.; Henderson, C. L. Thin Solid Films 2004, 449, 231.
37. D'Amour, J. N.; Okoroanyanwu, U.; Frank, C. W. Microelectron Eng 2004, 73/74, 209.
38. Dalnoki-Veress, K.; Forrest, J. A.; Murray, C.; Gigault, C.; Dutcher, J. R. Phys Rev E: Stat Phys Plasmas Fluids Relat Interdiscip Top 2001, 63, 031801.
39. Tompkins, H. G.; McGahan, W. A. Spectroscopic Ellipsometry and Reflectometry—A User's Guide; Wiley: New York, 1999.
40. Grohens, Y.; Brogly, M.; Labbe, C.; David, M.-O.; Schultz, J. Langmuir 1998, 14, 2929.
41. Hannon, M. J.; Koenig, J. L. J Polym Sci Part A-2: Polym Phys 1969, 7, 1085.
42. Arwin, H.; Aspnes, D. Thin Solid Films 1984, 113, 101.
43. Heavens, S. Optical Properties of Thin Solid Films; Dover: New York, 1991.
44. Fryer, D. S.; Nealey, P. F.; de Pablo, J. J. Macromolecules 2000, 33, 6439.
45. Brandrup, J.; Immergut, E. H.; Grulke, E. A., Eds. Polymer Handbook, 4th ed.; Wiley-Interscience: New York, 1999.
46. Wunderlich, W. Physical Constants of Poly(methyl methacrylate), 2nd ed.; Wiley: New York, 1975.
47. Moreau, W. M. Semiconductor Lithography; Plenum: New York, 1988; p 134.